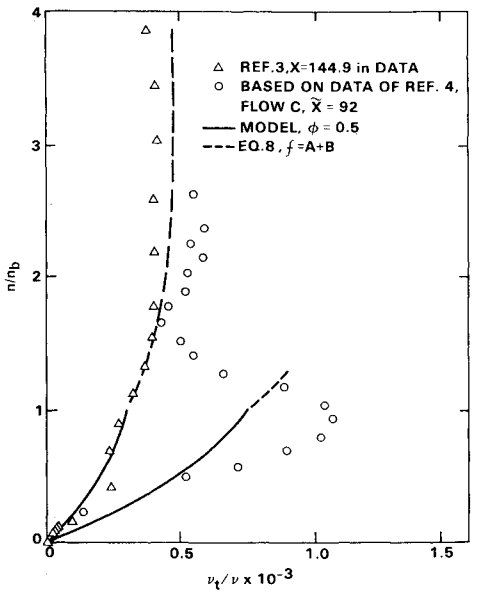

Fig. 3 Comparison between prediction and data of Refs. 4 and 3 for eddy viscosity.

where

$$\beta \equiv k_v/k_b = 1 + [(n_v/n_b)^2 - 1]\phi/(e^{\phi} - 1) \qquad (7b)$$

Thus L is proportional to n_v, increasing as the backflow develops and decreasing toward reattachment, in agreement with observations a and b.

An eddy viscosity formula is now obtained from the following argument. As pointed out in Ref. 5, the basic relation $\nu_t = C_\mu k^2/\epsilon$ must be modified within the viscous sublayer to preserve the correct behavior $\nu_t \sim n^3$ at the wall, giving rise to the formula $\nu_t = C(n)k^2/(\epsilon n^+)$. In a similar manner, eddy viscosity within the backflow is assumed to be of the form $\nu_t = f(n)k^2/\epsilon$. Using Eqs. (1-5), and (7) yields

$$\nu_t/\nu_w = [f(n/n_b)/(2\sqrt{2}\beta^2)]\, n_v^* \mathcal{G}^{1/2}(s,n), \quad 0 \le n \le n_b \qquad (8)$$

where

$$f(n/n_b) = A(n/n_b) + B,\ A = -(C_\mu^*/2)^{9/5},\ B = (C_\mu^*/2)^{3/5} - A$$

This form of f seems to best correlate with the data.[3,4]

The corresponding formula within the viscous sublayer is of the form $(\nu_t/\nu_w)_{\text{sub}} = C(n)[k^2/\nu\epsilon]_{\text{sub}}$, where k is given by Eq. (6) and $\epsilon = k_v^{3/2}/n_v$. Here, $C(n_b) = C_\mu^{*1/4}(A+B)/2\sqrt{2}$, A and B being given previously.

This concludes the formulation of the model, which ignores the viscous region adjacent to the wall within the separation bubble. This is justifiable in view of observation c.

Testing of Model

In order to test the model, arbitrary streamwise locations were selected from Ref. 4, flow C, $\tilde{x} = 92$, and from Ref. 3, $x = 144.9$ in. The two sets of data pertain to different geometries, initial conditions, and means by which flow separation was imposed. A large separation bubble existed in the flow of Ref. 4, and the chosen location is approximately in the middle of it. Figure 2 compares k from Eqs. (1) and (6), with the data. The agreement supports the Gaussian concept. Furthermore, calculated values of k_b at this and other locations were found to be within only 2% of those obtained from the measurements. Based on the measured velocity profile and shear stress distribution at the selected station, eddy-viscosity data were compared with Eq.(8), as shown in Fig. 3. Since the velocity profile had to be numerically treated to derive $\partial u/\partial y$, some error was introduced into the data points; nevertheless, the agreement is reasonable. In the case of Ref. 3, eddy viscosity was already given in data form. Figure 3 also shows comparison of ν_t prediction with these data at the selected location. Agreement is very good, even well beyond the backflow. In addition, predicted ν_t levels dropped about 45% when going from well upstream of separation into the bubble along a constant n, as experimentally observed.[3] This leads credibility to the length scale L. These tests serve as a preliminary validation of the model.

A parametric study showed that $\phi = 0.5$ is the best choice; this value is adopted as a constant of the model.

Conclusions

A k-ϵ formulation has been developed for turbulence modeling within wall-bounded two-dimensional separation bubbles. The model is based on experimental obsevations. Two basic features of the model are: 1) turbulence kinetic energy within the backflow region is a Gaussian function of the distance from the wall; 2) the length scale of turbulence within the bubble is proportional to the local distance from the wall to the edge of the viscous sublayer located outside the backflow region. The formulation enables unified k-ϵ modeling between the wall and the viscous sublayer edge.

The model has been preliminarily validated through comparisons with data, and will be incorporated into a Reynolds-averaged Navier-Stokes solver to calculate flowfields where separated regions may occur.

References

[1]Simpson, R. L., "Some Features of Two-Dimensional Turbulent Separated Flows," AIAA Paper 85-0178, Jan. 1985.

[2]Simpson, R. L., "A Review of Some Phenomena in Turbulent Flow Separation," *Transactions of ASME*, Vol. 103, Dec. 1981, pp. 520-533.

[3]Simpson, R. L., Chew, Y.-T., and Shivaprasad, B. G., "The Structure of a Separating Turbulent Boundary Layer. Part 1, Mean Flow and Reynolds Stresses," *Journal of Fluid Mechanics*, Vol. 113, Dec. 1981, pp. 23-51.

[4]Délery, J. M., "Experimental Investigation of Turbulence Properties in Transonic Shock/Boundary-Layer Interations," *AIAA Journal*, Vol. 21, Feb. 1983, pp. 180-185.

[5]Gorski, J. J., "A New Near-Wall Formulation for the k-ϵ Equations of Turbulence," AIAA Paper 86-0556, Jan. 1986.

Measurement of the Speed of Sound in Ice

Alphonso C. Smith*and Doron Kishoni†
NASA Langley Research Center, Hampton, Virginia

Introduction

SOUND-speed measurements in refrigerated ice have been determined by using pulse-echo ultrasonic applications. For these measurements, two parameters were important for accuracy, namely, the ice thickness and the time required for

Received Feb. 11, 1986; revision received March 27, 1986.

*Research Scientist, Instrument Research Division.
†NRC Research Associate.

the reflected echoes of the sound wave to travel through aluminum and ice and return to the transducer. The ice thickness was forced to be a known parameter by using an assembly of aluminum blocks with smooth surfaces and a trough for holding water. Time intervals between reflected echoes were obtained from an oscilloscope trace showing the echo signals for each interface at which the sound wave interacted. Data were obtained for both compressional and shear wave measurements using transducers with a diameter of 12.7 mm and 5-MHz central frequency operating range.

This research was initiated to examine the possibilities of using an ultrasonic transducer as an ice detector on critical surfaces such as aircraft wings, engines, and propellers. For this technique to be used, adequate and reliable data will be needed for sound speeds in ice in a variety of conditions. Aircraft fly in various atmospheric conditions, sometimes encountering severe weather where the liquid water content and temperature are such that icing can occur on critical surfaces. Ice formed at various conditions can have different sound speeds because sound speed is related to density and the elastic constants of a media.[1,2] The density[1] for pure ice at 0°C and 1 atm has been reported to be 0.9168 g/cm^{-3}. Ice containing air bubbles can have lower densities and, therefore, have a different sound speed than pure ice.

Recent studies[3,4] have been supported by the Federal Aviation Administration to gather atmospheric icing data to be used to help establish atom characterization of supercooled clouds up to 10,000 ft above ground level. The data from these reports were intended to serve as a basis for the establishment of design criteria and regulations that pertain to ice protection systems and equipment for low-performance aircraft, which typically operate below 10,000 ft. In Ref. 5, issues have been raised as to the sophistication, complexity, and expense involved in trying to equip aircraft with ice protection systems. Aircraft manufacturers have found that the development of ice protection systems, as well as adding extra weight, is very expensive for large aircraft. It would appear that an ultrasonic ice detection system would have to be low-weight and relatively inexpensive to be attractive for use in aircraft. An ultrasonics ice-detection warning system would serve to let pilots know when they are encountering an icing condition.

Some work has been initiated to study ice-detection systems.[6,7] In Ref. 6, a microwave ice detection system is discussed. In Ref. 7, Hansman and Kirby detailed measurements they made using compressional sound waves to detect ice accretion under different icing conditions. Their work was done using a mechanical measurement to determine the ice thickness, where the top reflection echo surface of the ice was open and irregular. The studies in this report will focus on making sound-speed measurements with a well-defined ice thickness. Data were obtained in a laboratory-controlled environment for both compressional and shear sound waves for a well-defined ice thickness using a trough to confine the ice to a known width.

Experimental Procedure and Results

All measurements were made using ultrasonic techniques operating in a pulse-echo mode. Carefully machined aluminum blocks were fabricated to the dimensions given in Fig. 1. Final dimensions of the blocks and trough width were determined from a micrometer measurement. The aluminum blocks were machined with a trough of a known width for holding water that could be placed in a refrigerator. With ice in the trough at −26°C and at a fixed width, sound-speed measurements were determined from oscilloscope traces showing echo reflections at the aluminum/ice and ice/aluminum interfaces. All the aluminum surfaces in the path of the sound beam were machined to a 32 microfinish to give good transmission and reflection characteristics. Multiple-reflection echoes were obtained at all the interfaces, and the reflection echoes were spaced according to the travel time in the medium. The travel time of the sound wave through the ice

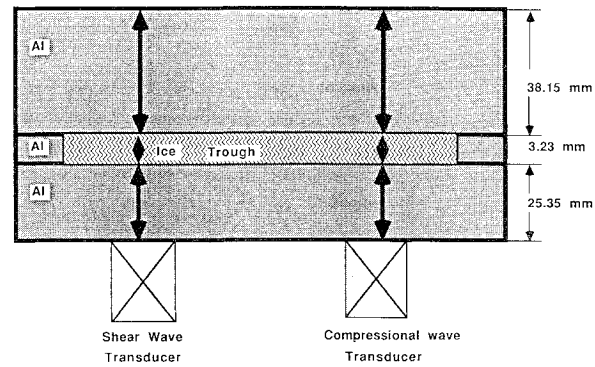

Fig. 1 Schematic drawing of aluminum blocks used for sound-speed measurements in ice with a known trough width. Water was used in the trough for evaluation purposes before the assembly was placed in a refrigerator for testing at −26°C.

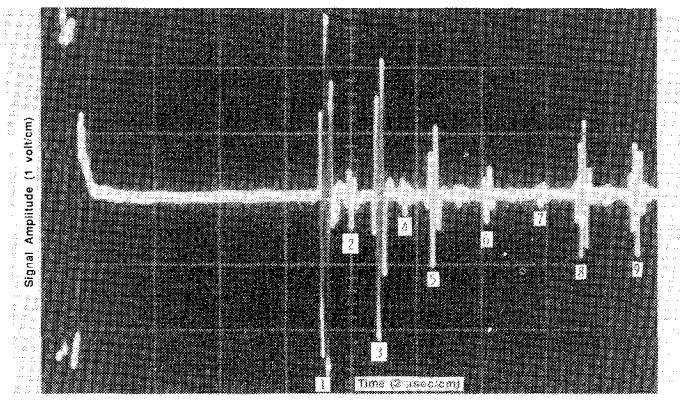

Fig. 2 Oscilloscope trace showing compressional wave echoes from the aluminum/ice, 1 and 8; ice/aluminum, 3, 5, 6, 7, and 9 interfaces. ΔT between 1 and 3, 3 and 5, 5 and 6, 7 and 7, 8 and 9 was 1.64 μs. ΔT between 1 and 8 was 8.08 μs, between 1 and 9, 9.72 μs. The echoes at 2 and 4 could not be accounted for and were assumed to be caused by defects or inclusions in the ice, such as cracks or air bubbles.

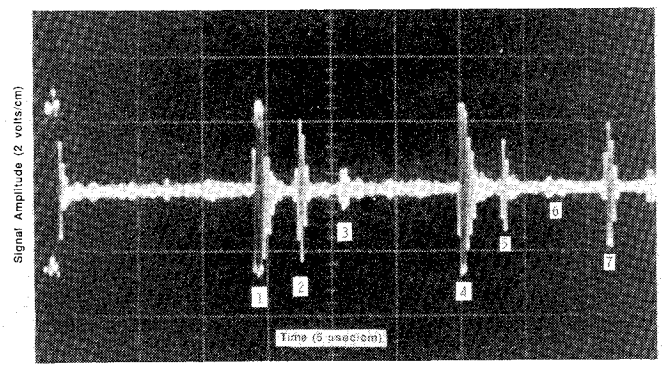

Fig. 3 Oscilloscope trace showing shear wave echoes from the aluminum/ice 1 and 4; ice/aluminum, 2, 3, 5, and 6; and aluminum/air, 7 interfaces. ΔT between echoes 1 and 2, 2 and 3, 4 and 5, 5 and 6 was 3.25 μs. ΔT between echoes 1 and 4, 2 and 7 was 16.24 μs and 23.8 μs, respectively.

was determined from the time difference in the reflected echoes appearing on the oscilloscope trace from the aluminum/ice and ice/aluminum interfaces.

In Fig. 2, echo reflections are shown for a compressional wave with ice in the trough of Fig. 1. The separation time between reflections 1 and 3, 3 and 5, 5 and 6, 6 and 7, 8, and 9, represents how long it took for the compressional sound wave to travel through the ice. In the pulse-echo operational mode, the sound speed in a material is equal to twice the thickness

divided by the separation time between adjacent echo reflections. The reflected echo separation times were determined to be 1.64 μs to give a speed of sound for a compressional wave in glaze ice of 3.94 mm/μs. This compares favorably with the results obtained in Ref. 7. The time separation between echoes 1 and 9 was 9.72 μs and corresponds to the travel time of the compressional wave through the front piece of aluminum and the ice trough. In Fig. 3, results are shown that give multiple echoes for shear waves coupled into the ice. The time difference between echoes 1 and 2, 2 and 3, 4 and 5, 5 and 6, represents how long it took for the shear wave to travel through the ice. The time was determined to be 3.25 μs. For a trough width of 3.23 mm, this gave a shear sound speed of 1.99 mm/μs in ice. This measurement gives a shear sound speed in ice of approximately one-half that for a compressional wave.

Concluding Remarks

Data are given to show how sound-speed measurements in refrigerated ice were determined using both compressional and shear waves. Oscilloscope traces were obtained using pulse-echo ultrasonics experimental procedures. Two parameters were needed to determine sound speeds in ice using this technique. These parameters were the ice thickness and the time of travel of the sound wave through ice. The time measurements were obtained from an oscilloscope trace using time cursor markers with trace overlapping ability and digital time readout on the oscilloscope screen. The ice thickness was forced to be a known value by machining a trough in an aluminum block. All surfaces of the aluminum blocks coming in contact with the sound beam were machined to a smooth 32 microfinish to assure good transmission and reflection of the sound waves at the aluminum interfaces. Clear and sharp echo reflections were obtained for both compressional and shear waves at the aluminum/ice and ice/aluminum interfaces. The geometry chosen permits accurate determination of sound speeds in ice through the use of a known ice thickness and smooth surfaces in the sound beam path. Typically, the top surface of ice formed while exposed to air will not be smooth and flat. This can contribute to mode conversions and other echo reflcetion variations. The type of geometry and surface preparation chosen ensures that the ice surfaces interacting with the sound beam will be bonded to a smooth surface.

The work presented in this report was done at one ice temperature. It is recognized that the properties of ice can vary, depending on certain environmental conditions. Ice formed at various conditions can have different sound speeds depending on the density and elastic constants. The sound speeds in ice reported here are expected to be good for the conditions given: refrigerated ice at $-26°C$.

References

[1]Ponder, E.R., *The Physics of Ice,* Pergamon Press, Elmsford, NY, 1965, pp. 107-115.

[2]Filipczynski, L., Pawlowski, Z., and Wehr, J. Jr., *Ultrasonic Methods of Testing Materials,* Butterworth, London, 1966, pp. 12-15.

[3]Jeck, R.K., "A New Data Base of Supercooled Cloud Variables for Altitudes up to 10,000 Feet AGL and the Implications for Low Altitude Aircraft Icing," NRL Report 8738, Aug. 1983.

[4]Masters, C.O., "A New Characterization of Supercooled Clouds Below 10,000 Feet AGL," Rept. DOT/FAA/CT-83/22, June 1983.

[5]Flight Safety Research Branch, ACT-340, "Engineering and Development Program Plan-Aircraft Icing," Rept. DOT/FAA/CT-83/7, Aug. 1983.

[6]Magenheim, B. and Rocks, J.K., "Developement and Test of a Microwave Ice Accretion Measurement Instrument (MIAMI)," NASA CR-3598, 1982.

[7]Hansman, R.J. Jr. and Kirby, M.S., "Measurements of Ice Accretion Using Ultrasonic Pulse-Echo Techniques," *Journal of Aircraft,* Vol. 22, June 1985, PP. 530-535.

Noninvasive Experimental Technique for the Measurement of Unsteady Velocity Fields

L. Lourenco* and A. Krothapalli†
Florida State University, Tallahassee, Florida
and
J.M. Buchlin‡ and M.L. Riethmuller‡
von Kármán Institute for Fluid Dynamics
Rhode-St-Genese, Belgium

Introduction

ONE of the difficult problems in experimental fluid mechanics remains the measurement of velocity and vorticity fields in unsteady flows. Current methods for the measurement of vorticity involve the use of multiple hot-wire anemometers or laser Doppler velocimeters to independently measure the components of the velocity vector at closely spaced locations. The "local" flow vorticity is then determined by applying a finite-difference scheme to the measured velocity components. However, these techniques suffer from some drawbacks. First, the presence of several hot-wire probes in a small region of the flow produces significant blockage effects that perturb the local flow pattern. Second, in most cases, the distance between the multiple measuring volumes is not small enough to accurately resolve the local velocity gradients. This results in "spatially filtered" vorticity estimates. Third, these methods can provide only "one-point" information. In order to obtain data on the entire field, measurements must be carried out sequentially one point at a time. Although this sequential procedure can be easily implemented to investigate steady flows, it is rather difficult to use in unsteady flows.

When a global and instantaneous picture of the flowfield is required, researchers rely heavily on various flow visualization techniques. Traditionally, flow visualization pictures have been used to qualitatively study global flow properties. However, with the advent of fast computers, capable of handling high-resolution images, it is now possible to combine advanced visualization techniques with digital processing algorithms to obtain quantitative information.

This note presents a new technique known as particle image displacement velocimetry, which permits the visualization of two-dimensional flows as well as the quantification of the instantaneous velocity and vorticity fields.

Principle of the Technique

The principle of operation of particle image displacement velocimetry (PIDV) is sketched on Fig. 1. It involves two equally important steps. In the first step, a plane of the flow seeded with small particles is recorded (Fig. 1a). A sheet of light produced by a laser source illuminates a selected plane of the flow. A pulsed laser, such as a ruby or a NdYag laser, or a continuous wave (CW) laser with a shutter device, is used as the light source. The light scattered by the seeding particles in the illuminated plane provides a moving pattern. For low seeding concentrations, this pattern consists of resolved dif-

Received Nov. 12, 1985; revision received Jan. 24, 1986.

*Assistant Professor of Mechanical Engineering, FAMU/FSU College of Engineering. Member AIAA.
†Associate Professor of Mechanical Engineering, FAMU/FSU College of Engineering. Member AIAA.
‡Associate Professor.